Journal of Systems Engineering and Electronics
Vol. 32, No. 3, June 2021, pp.566 – 572

Research on LPI radar signal detection and parameter estimation technology

WAN Tao*, JIANG Kaili, LIAO Jingyi, JIA Tingting, and TANG Bin

School of Information and Communication Engineering, University of Electronic Science and Technology of China, Chengdu 611731, China

Abstract: Modern radar signals mostly use low probability of intercept (LPI) waveforms, which have short pulses in the time domain, multicomponent properties, frequency hopping, combined modulation waveforms and other characteristics, making the detection and estimation of LPI radar signals extremely difficult, and leading to highly required significant research on perception technology in the battlefield environment. This paper proposes a visibility graphs (VG)-based multicomponent signals detection method and a modulation waveforms parameter estimation algorithm based on the time-frequency representation (TFR). On the one hand, the frequency domain VG is used to set the dynamic threshold for detecting the multicomponent LPI radar waveforms. On the other hand, the signal is projected into the time and frequency domains by the TFR method for estimating its symbol width and instantaneous frequency (IF). Simulation performance shows that, compared with the most advanced methods, the algorithm proposed in this paper has a valuable advantage. Meanwhile, the calculation cost of the algorithm is quite low, and it is achievable in the future battlefield.

Keywords: multicomponent signals detection, parameter estimation, visibility graphs (VG), low probability of intercept (LPI), time-frequency representation (TFR).

DOI: 10.23919/JSEE.2021.000048

1. Introduction

In the contemporary battlefield environment, the interception and sensing of non-cooperative parties are mostly low probability of intercept (LPI) radar signals, which use special transmission waveforms to prevent the sensing of non-cooperative parties [1]. LPI radar waveforms generally have the characteristics of short pulses in the time domain, agile waveforms in the pulse, rapid agile beams, combined modulation waveforms, and simultaneous arrival of multiple signals [2], which makes signal sensing by non-cooperative parties particularly difficult. Therefore, the research on signal sensing of LPI radar plays a critical role in the maintenance of military applications.

Considered in a complex electromagnetic environment, multiple LPI radar waveforms are input at the same time, and the signal detection performance will deteriorate. In the past LPI radar signal detection algorithms, two-dimensional representation [3−5], cyclic shifting [6], autocorrelation, and other algorithms [7] are used, and they have achieved good performance. However, these algorithms hardly consider the detection of multicomponent signals, which is inseparable from practical applications. In [8], an algorithm to convert from time series to visibility graphs (VG) was proposed. This paper uses the statistical characteristics of the frequency domain VG to set the dynamic threshold based on the Neyman Pearson criterion (NYC), and then the corresponding signal detection probability is obtained.

Parameter estimation has long been a question of great interest in a wide range of signal processing [9]. In [10,11], frequency hopping parameter estimation based on machine learning and sparse Bayes was proposed. In [12−15], the time-frequency representation (TFR) method for frequency estimation was introduced. In [16,17], the parameters of the frequency shift keying (FSK)/binary phase shift keying (BPSK) combined modulation waveform were estimated, and the performance is superior. Instantaneous frequency (IF) estimation, which describes the law of signal frequency changing with time, is the foundation of the time-frequency analysis domain. Therefore, many researchers consider estimating IF from the perspective of TFR [18]. Also, adaptive TFR is also a current research hotspot [19,20]. The common point of these methods is to reassign each point to the center of gravity located in its vicinity. Moreover, the positioning of signal components in the time-frequency (TF) domain can be improved while suppressing interference terms. In

Manuscript received July 11, 2020.
*Corresponding author.
This work was supported by the National Defence Pre-research Foundation of China (30502010103).

[21−25], an adaptive short-time Fourier transform (STFT) algorithm was proposed to determine the window width by analyzing the IF gradient, and estimate simultaneously the IF of the signal by detecting the ridges of the wavelet transform. Reference [26] is also to optimize the window width to obtain the best case in TFR, thereby minimizing the estimated value of the mean square error (MSE) at each position in the time-frequency domain.

This paper proposes a TFR-based FSK/BPSK symbol width and IF joint parameter estimation algorithm. First, the FSK/BPSK waveform is represented by smooth pseudo-Wigner Ville distribution (SPWVD), and then the symbol width and IF are estimated by performing time-domain and frequency-domain projections, respectively. The innovation of this paper lies in the proposed LPI radar signal parameter estimation method based on time-frequency representation projection. Moreover, the VG-based multicomponent LPI radar signal detection algorithm is also proposed for the first time. Further, the signal detection probability and the parameter estimation accuracy of FSK/BPSK signals are greatly improved compared with the state-of-the-art technology.

The remaining paper is structured as follows. Section 2 provides an overview of the multicomponent signal detection model. Section 3 describes the parameter estimation of the FSK/BPSK combined modulation waveform. Section 4 presents the validation of the proposed algorithm including the simulation experiment setup, results, and discussion. Section 5 concludes the paper and presents the potential future research directions.

2. Multicomponent signal detection model

Considering a signal sensing environment, electronic warfare (EW) receivers intercept three signals from different directions simultaneously in the air, and their signal strengths are different, then [27,28]

$$y_1[k] = x_1[k] + n_1[k] = b_1 \exp\{\mathrm{j}[2\pi f_1[k](kT_s) + \varphi_1[k]]\} + n_1[k], \quad (1)$$

$$y_2[k] = x_2[k] + n_2[k] = b_2 \exp\{\mathrm{j}[2\pi f_2[k](kT_s) + \varphi_2[k]]\} + n_2[k], \quad (2)$$

$$y_3[k] = x_3[k] + n_3[k] = b_3 \exp\{\mathrm{j}[2\pi f_3[k](kT_s) + \varphi_3[k]]\} + n_3[k], \quad (3)$$

$$y[k] = y_1[k] + y_2[k] + y_3[k] \quad (4)$$

where $\{b_1, b_2, b_3\}$, $\{f_1, f_2, f_3\}$, $\{\varphi_1, \varphi_2, \varphi_3\}$ are respectively the random amplitude, carrier frequency, and phase of the original signal $\{x_1, x_2, x_3\}$, k is the sample index for each T_s increasing with the sampling frequency f_s, under a given pulse time interval τ_{pw}, $0 \leqslant kT_s \leqslant \tau_{pw}$, $\{n_1[k], n_2[k], n_3[k]\}$ is additive white Gaussian noise (AWGN), and y is the sum of the signals received by the EW receiver as $\{y_1, y_2, y_3\}$.

A VG is an undirected graph for a time-ordered sequence $S = \{y_1, y_2, \cdots, y_n\}$. Assume that three arbitrary nodes i, j, k are labeled corresponding to data y_i, y_j and y_k, respectively. The two nodes i and j (assume $i < k < j$ without loss of generality) are connected, if and only if one straight line can connect y_i and y_j, without any intersecting intermediate data y_k. Then there is

$$y_k < y_i + \frac{k-i}{j-i}(y_j - y_i), \ \forall k : i < k < j. \quad (5)$$

They satisfy three criteria: (i) Each vertex is connected to at least two adjacent points. (ii) The connection relationship is non-directional. (iii) VG has rotation invariance, no matter whether its signal amplitude and sampling frequency are changed at the same time or not, the connection relationship remains unchanged [8].

Taking six-time instants as an example, the corresponding signal amplitude and the connection relationship of the VG sequence are shown in Fig. 1. VG means if you can see the surrounding points at a certain point, a connection relationship is established; otherwise, it is irrelevant, and there is no connection relationship.

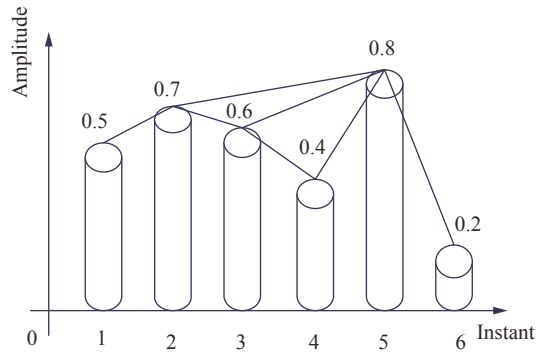

Fig. 1 An illustration of N=6 instants versus signal amplitude between 0-1 for the VG algorithm

When the false alarm probability is set to $P_f = P(H_1|H_0) = \alpha$ by the VG statistical average value in the frequency domain of the signal, according to NYC, the detection probability can be expressed as $P_d = P(H_1|H_1)$. Using Lagrange multiplier $\mu(\mu \geqslant 0)$, construct the objective function as

$$J = P_d - \mu[P_f - \alpha] = P(H_1|H_1) - \mu[P(H_1|H_0) - \alpha]. \quad (6)$$

To maximize the detection probability P_d,

$$J=\int_{R_1}p(H_1|H_1)\mathrm{d}y-\mu\int_{R_1}p(H_1|H_0)\mathrm{d}y+\mu\alpha=\int_{R_1}[p(H_1|H_1)-\mu p(H_1|H_0)]\,\mathrm{d}y+\mu\alpha. \tag{7}$$

Since $\mu\geqslant 0$, $p(H_1|H_1)-\mu p(H_1|H_0)\geqslant 0$, from which the likelihood ratio function can be constructed.

$$L(y)=\frac{p(H_1|H_1)}{p(H_1|H_0)}\underset{H_0}{\overset{H_1}{\gtrless}}\mu \tag{8}$$

To satisfy the condition of $p(H_1|H_0)=\alpha$, μ should be satisfied.

$$p(H_1|H_0)=\int_{R_1}p(H_1|H_0)\mathrm{d}y=\int_{\mu}^{\infty}p(L|H_0)\mathrm{d}L=\alpha \tag{9}$$

Therefore, given an α, it corresponds to a detection threshold μ, and then the detection probability P_d is determined according to this threshold.

3. Parameter estimation of FSK/BPSK combined modulation waveform

The FSK/BPSK waveform is usually a combination of two modulation modes: FSK and BPSK. FSK/BPSK combined modulation waveform can be expressed as

$$s(n)=A\sum_{k=1}^{M}\exp[\mathrm{j}(2\pi f_k n+\theta(n))]\,\mathrm{rect}[n-(k-1)T_b] \tag{10}$$

where A is the amplitude of the signal, $\mathrm{rect}(n)$ is the rectangular pulse, T_b is the symbol width, M is a positive integer, f_k is the frequency encoding information at time $[kT_b,(k+1)T_b]$, and $\theta(n)=\pi d(n)$ is the phase encoding, $d(n)=\{0,1\}$. BPSK has a lower side lobe and Doppler tolerance than a single pulse. Due to the problem of frequency modulation sequence, FSK avoids the reactive interference of the jammer to the transmission frequency [1]. FSK/BPSK takes into account the performance of both and has a lower interception.

This paper proposes an SPWVD-based FSK/BPSK combined modulation waveform parameter estimation method. SPWVD [29−31] can be expressed as

$$\mathrm{SPW}_x(t,\omega)=\int h(\tau)\int g(s-\omega)x(t+\tau/2)x^*(t-\tau/2)\mathrm{e}^{-\mathrm{j}\omega\tau}\mathrm{d}s\mathrm{d}\tau \tag{11}$$

where $h(t)$ represents the window function, $g(t)$ represents the smoothing function, $x(t)$ represents the signal itself, and $\mathrm{SPW}_x(t,\omega)$ represents the TFR obtained by the SPWVD transformation of the signal. This method first converts the LPI radar signal into a time-frequency image, and then projection in the time and frequency domains are performed, separately. Next, the symbol width and carrier frequency rate f_k are calculated. The more specific processing and the corresponding simulation are shown in Fig. 2.

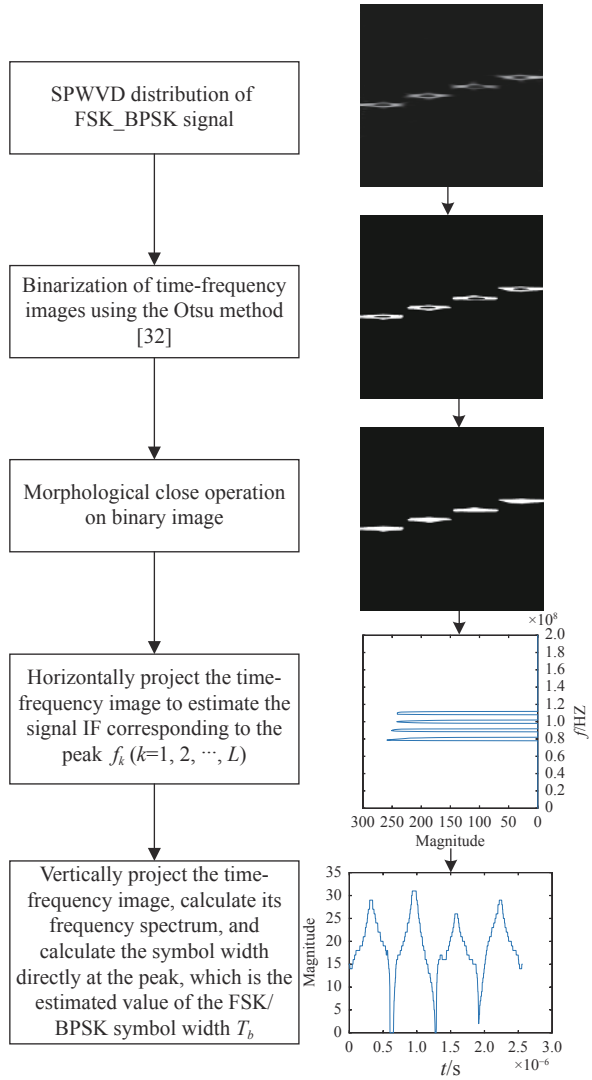

Fig. 2 Flow chart of the FSK/BPSK signal parameter estimation method based on SPWVD

4. Simulation performance evaluation

4.1 Parameter setting

The experimental parameters include all parameter settings of the LPI radar waveform. The sampling frequency f_s is 400 MHz, the f_0 signal frequency is 80 MHz, the code rate f_b is 10 MHz, the number of symbols N is 4, the duration τ_{pw} is N/f_b, the symbol rate of FSK is $\{10,20,30,40\}\times 10^6$ respectively, and the phase of BPSK is $(0,\pi)$.

4.2 Multicomponent detection performance

Given each signal has its VG, the VGs are different even

under the same signal-to-noise ratio (SNR). Therefore, the statistics of VG can be considered as the basis for judging the probability of NYC false alarm. In this paper, by setting the density of the VG median to 1 as the basis for NYC judgment, the constant false alarm probability P_f is set to 0.005, and the performance of the 1 000-time Monte Carlo algorithm is shown in Fig. 3.

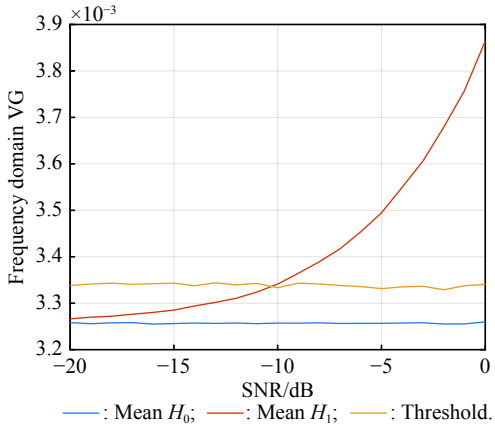

Fig. 3 Multicomponent signal parameter estimation

It can be seen from Fig. 3(a) that when the SNR is low, the average frequency density H_1 and H_0 of 1 000 independent experiments are close to each other. As the SNR increases, the average frequency density H_1 gradually increases, and the average frequency density of H_1 gradually increases. As shown in Fig. 3(b), when SNR>−7 dB, the correct detection probability of the signal is more than 90%, when the SNR is −3 dB, the signal correct detection probability is approximatively 100%. Since this paper is a multicomponent LPI radar waveform detected, the detection probability is lower than that of a single signal. The environment setting is consistent with [3,7], the performance comparison experiment is shown in Fig. 4.

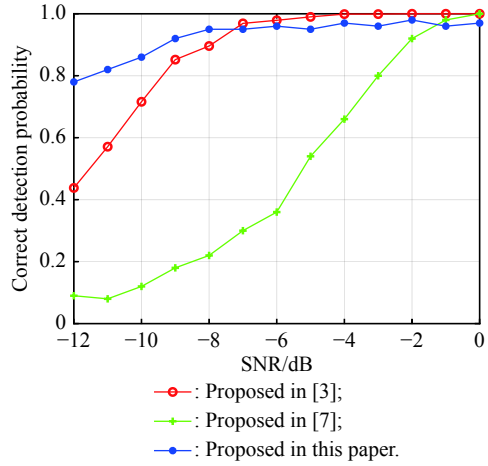

Fig. 4 Comparison experiment of signal detection

Through comparative experiments, it can be found that the algorithm proposed in this paper is slightly weaker at low SNRs [3]. However, with the increase of SNR, especially after SNR>−5 dB, the correct detection probability is already close to 100%, which has certain advantages over the literature [3] and [7]. The algorithm proposed in this paper simultaneously is more suitable for a complex electromagnetic environment.

Considering the different constant false alarm probabilities, set P_{fa} to be 0.001, 0.005, 0.01, 0.05, and 0.1 respectively, and the corresponding detection probabilities are shown in Fig. 5. It is easy to find that when SNR< −10 dB, except for the case where P_{fa} is 0.1, the signal detection probabilities of the other four cases are all less than 0.8. However, the signal detection probability increases with the increase of SNR in all P_{fa} cases, which is consistent with our cognition. When SNR>−5 dB, the correct detection probability of multicomponent signals is close to 100%.

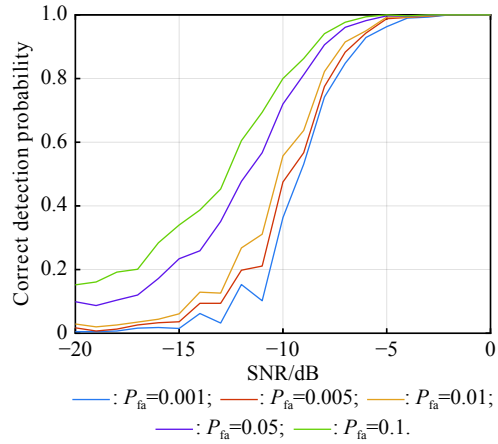

Fig. 5 Multicomponent signal detection probability under different false alarm probabilities

4.3 Performance of FSK/BPSK combined modulation parameter estimation

For combined FSK/BPSK waveforms, the conventional parameter estimation method generally removes the BPSK by squaring the signal, which reduces the SNR by 3 dB, therefore the parameter estimation accuracy is weak in the case of low SNRs. In this paper, the parameter estimation of the FSK/BPSK combined modulation waveform does not require signal squaring. In this way, the accuracy of the parameter estimation can be ensured at low SNRs.

The setting environment is consistent with those in [16,17]. Normalized root-mean-square error (NRMSE) is used as the basis for performance comparison. The 500 times Monte Carlo simulation is shown in Fig. 6. It is easy to find that the algorithm proposed in this paper has a better IF estimation performance at low SNRs, which is consistent with the previous analysis. The LPI radar signal after SPWVD representation can also show its superior energy gathering performance at low SNRs. Therefore, compared to [16,17], the algorithm proposed in this paper performs better in IF estimation performance under low SNRs. With the increase of SNR, the improvement of energy aggregation is no longer so obvious. The maximum point found by the projection algorithm is not significantly improved from that under low SNRs, but it can still maintain high estimation performance.

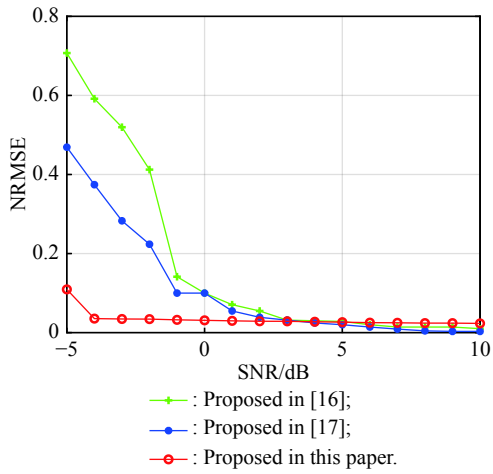

Fig. 6 Frequency overlap parameter estimation situation

However, the algorithm proposed in this paper has certain limitations. Since it is a projection calculation when the frequency overlaps, only one value can be estimated, and the peak calculation error will increase. As shown in Fig. 7, when SNR is 0 dB, IF projection and code element width projection can be used. It can be found that when frequency overlap occurs, several frequency division signals can be judged from the code element width projection diagram alone. Then feedback to the IF projection diagram to find out the highest point of energy and judge the position corresponding to the highest point of frequency overlap. However, in this way, if the frequency overlaps too much, it is not easy to calculate the IF corresponding to each symbol width.

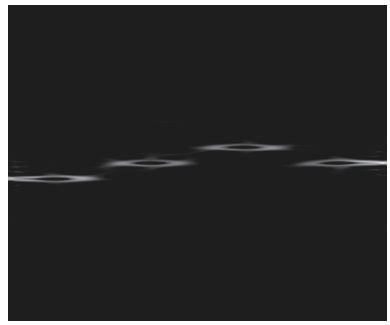

(a) Original time-frequency diagram

(b) Time-frequency diagram after binarization

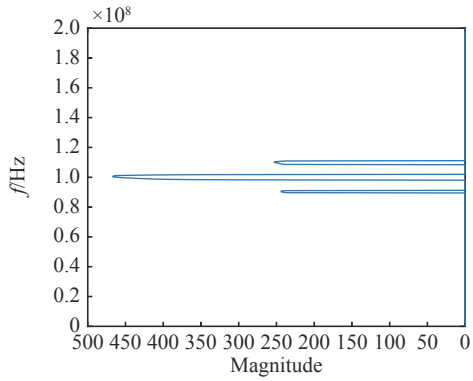

(c) IF projection

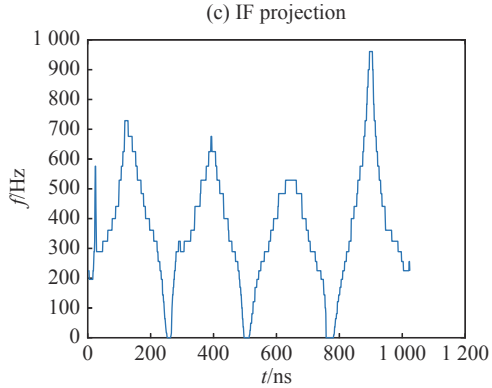

(d) Symbol broadband projection

Fig. 7 Comparison of symbol width estimation algorithms

The 500 Monte Carlo independent experiments are shown in Fig. 8. It can be found that the estimation accuracy of code element width parameters proposed in this paper is also higher than [16,17] at low SNRs, and the performance presents a very stable trend with the increase of SNRs. The code width estimation is similar to the IF estimation. In low SNRs, due to the good time-frequency energy aggregation, the estimated performance is very superior, and the estimated error is not very large. For example, when SNR is −5 dB, NRMSE is only 0.2, which is beyond the capability of most parameter estimation algorithms. With the increase of SNR, the time-frequency energy aggregation performance has not improved significantly, therefore, the performance growth of bit width estimation with SPWVD is also slowed down. Also, the fundamental reason for the parameter estimation error under high SNRs is that the image resolution is not high. For example, if the pixel is 128, each time the projection is different by one pixel, the error will increase by 1/128. Nevertheless, LPI radar signals are mainly faced with low SNR conditions. Therefore, it is reasonable to think that the algorithm proposed in this paper has certain advantages in the algorithm estimation of FSK/BPSK. Moreover, it can also be extended to other single signal parameter estimation. However, it still has some limitations, especially when the signal is sorted and the multicomponent signal needs to be estimated, the algorithm proposed in this paper is inaccurate in estimating the symbol width.

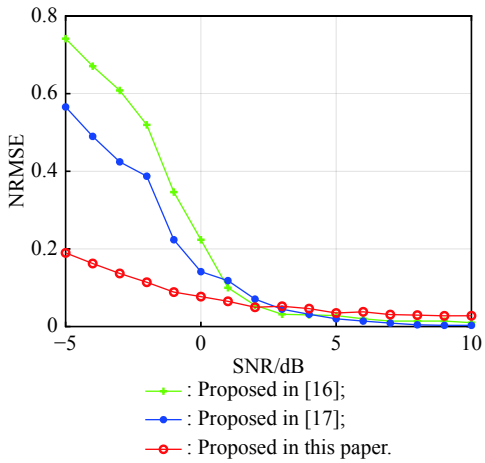

Fig. 8 Comparison of IF estimation algorithms

5. Conclusions

This paper presents an LPI radar signal detection and parameter estimation algorithm for passive radar, which is based on VG for multicomponent signal detection and SPWVD for FSK/BPSK parameter estimation. The simulation performance shows that the algorithm proposed in this paper is superior to the-state-of-the-art algorithm. Further, it is also more suitable for a complex electromagnetic environment. When SNR>−7 dB, the correct detection probability of the signal is more than 90%, and when SNR is −5 dB, the NRMSE of parameter estimation is only 0.2. However, the estimation algorithm still has weaknesses, such as the problem of parameter estimation accuracy of multicomponent signals when the signals are not sorted. Meanwhile, we believe that the algorithm proposed in this paper will play an important role in the future battlefield. In future work, we will consider multicomponent signal spectrum sensing and parameter estimation techniques.

References

[1] PACE P E. Detecting and classifying low probability of intercept radar. Norwood: Artech House, 2009.
[2] WILEY R G. ELINT: the interception and analysis of radar signals. Fitchburg: Artech House, 2006.
[3] KONOPKO K. A detection algorithm of LPI radar signals. Proc. of the Signal Processing Algorithms Architectures Arrangements and Applications, 2007: 103–108.
[4] GEROLEO F G, BRANDT-PEARCE M. Detection and estimation of LFMCW radar signals. IEEE Trans. on Aerospace and Electronic Systems, 2012, 48(1): 405–418.
[5] LIU Y J, XIAO P, WU H C, et al. LPI radar signal detection based on radial integration of Choi-Williams time-frequency image. Journal of Systems Engineering and Electronics, 2015, 26(5): 973–981.
[6] VLOK J D, OLIVIER J C. Non-cooperative detection of weak spread-spectrum signals in additive white Gaussian noise. IET Communications, 2012, 6(16): 2513–2524.
[7] YANG C Z, XIONG Z W, GUO Y, et al. LPI radar signal detection based on the combination of FFT and segmented autocorrelation plus PAHT. Journal of Systems Engineering and Electronics, 2017, 28(5): 890–899.
[8] LACASA L, LUQUE B, BALLESTEROS F, et al. From time series to complex networks: the visibility graph. Proceedings of the National Academy of Sciences, 2008, 105(13): 4972–4975.
[9] POOR H V. An introduction to signal detection and estimation. Berlin: Springer Science & Business Media, 2013.
[10] KO C C, ZHI W, CHIN F. ML-based frequency estimation and synchronization of frequency hopping signals. IEEE Trans. on Signal Processing, 2005, 53(2): 403–410.
[11] ZHAO L F, WANG L, BI G A, et al. Robust frequency-hopping spectrum estimation based on sparse Bayesian method. IEEE Trans. on Wireless Communications, 2014, 14(2): 781–793.
[12] KHAN N A, BOASHASH B. Multicomponent instantaneous frequency estimation using locally adaptive directional time frequency distributions. International Journal of Adaptive Control and Signal Processing, 2016, 30(3): 429–442.
[13] DONG X J, CHEN S Q, XING G P, et al. Doppler frequency estimation by parameterized time-frequency transform and phase compensation technique. IEEE Sensors Journal, 2018, 18(9): 3734–3744.

[14] BEY A E, LINH-TRUNG N, ABED-MERAIM K, et al. Underdetermined blind separation of nondisjoint sources in the time-frequency domain. IEEE Trans. on Signal Processing, 2007, 55(3): 897–907.
[15] KHAN N A, MOHAMMADI M, DJUROVIC I. A modified Viterbi algorithm-based IF estimation algorithm for adaptive directional time-frequency distributions. Circuits, Systems, and Signal Processing, 2019, 38(5): 2227–2244.
[16] ZENG X D, ZENG D G, TANG B. Parameter estimation approach of 2FSK/BPSK hybrid signal based on ZAM-GTFR. Electronic Information Warfare Technology, 2011, 26(2): 9–14. (in Chinese)
[17] SONG J, LIU Y, WANG X D. The recognition and parameter estimation of hybrid modulation signal combined with FSK and BPSK. Journal of Electronics Information Technology, 2013, 35(12): 2868–2873. (in Chinese)
[18] STANKOVIC L. A measure of some time-frequency distributions concentration. Signal Processing, 2001, 81(2): 621–631.
[19] JIANG Q, SUTER B W. Instantaneous frequency estimation based on synchrosqueezing wavelet transform. Signal Processing, 2017, 138: 167–181.
[20] KWOK H K, JONES D. L. Improved instantaneous frequency estimation using an adaptive short-time Fourier transform. IEEE Trans. on Signal Processing, 2000, 48(10): 2964–2972.
[21] OBERLIN T, MEIGNEN S, PERRIER V. Second-order synchrosqueezing transform or invertible reassignment? Towards ideal time-frequency representations. IEEE Trans. on Signal Processing, 2015, 63(5): 1335–1344.
[22] FOURER D, AUGER F, CZARNECKI K, et al. Chirp rate and instantaneous frequency estimation: application to recursive vertical synchrosqueezing. IEEE Signal Processing Letters, 2017, 24(11): 1724–1728.
[23] MOHAMMADI M, POUYAN A A, KHAN N A, et al. Locally optimized adaptive directional time-frequency distributions. Circuits, Systems, and Signal Processing, 2018, 37(8): 3154–3174.
[24] BOASHASH B, OUELHA S. An improved design of high-resolution quadratic time-frequency distributions for the analysis of nonstationary multicomponent signals using directional compact kernels. IEEE Trans. on Signal Processing, 2017, 65(10): 2701–2713.
[25] ZHONG J G, HUANG Y. Time-frequency representation based on an adaptive short-time Fourier transform. IEEE Trans. on Signal Processing, 2010, 58(10): 5118–5128.
[26] ABDOUSH Y, POJANI G, CORAZZA G E. Adaptive instantaneous frequency estimation of multicomponent signals based on linear time-frequency transforms. IEEE Trans. on Signal Processing, 2019, 67(12): 3100–3112.
[27] WAN T, FU X Y, JIANG K L, et al. Radar antenna scan pattern intelligent recognition using visibility graph. IEEE Access, 2019, 7: 175628–175641.
[28] WAN T, JIANG K L, TANG Y L, et al. Automatic LPI radar signal sensing method using visibility graphs. IEEE Access, 2020, 8: 159650–159660.
[29] COHEN L. Time-frequency analysis. Upper Saddle River: Prentice Hall, 1995.
[30] RAVITEJA P, PHAN K T, HONG Y, et al. Interference cancellation and iterative detection for orthogonal time frequency space modulation. IEEE Trans. on Wireless Communications, 2018, 17(10): 6501–6515.
[31] YU G. A concentrated time-frequency analysis tool for bearing fault diagnosis. IEEE Trans. on Instrumentation and Measurement, 2019, 69(2): 371–381.
[32] NOBUYUKI O. A threshold selection method from gray-level histograms. IEEE Trans. on Systems, Man, and Cybernetics, 1979, 9(1): 62–66.

Biographies

WAN Tao was born in 1995. He received his B.S. degree from Harbin University of Commerce in 2017, Harbin, China. He is currently pursuing his Ph.D. degree with University of Electronic Science and Technology of China. He is interested in electronic reconnaissance and is mainly engaged in electronic countermeasures, signal processing and machine learning.
E-mail: taowan.uestc0939@foxmail.com

JIANG Kaili was born in 1991. She received her B.S. degree from University of Electronic Science and Technology of China (UESTC), Chengdu, China, in 2013. Currently, she is working toward her Ph.D. degree in the School of Information and Communication Engineering, UESTC. Her research interests include wideband spectrum sensing, sparse/compressive sensing and radar signal processing.
E-mail: jiangkelly@foxmail.com

LIAO Jingyi was born in 1996. She received her B.S. degree from University of Electronic Science and Technology of China (UESTC), Chengdu, China, in 2018. She is currently pursuing her M.S. degree with the School of Information and Communication Engineering, UESTC. Her research interest includes LPI radar signal detection and classification.
E-mail: LiaoJingyi@std.uestc.edu.cn

JIA Tingting was born in 1994. She received her B.S. degree from Kunming University of Science and Technology, Kunming, China, in 2017. She is currently pursuing her M.S. degree with University of Electronic Science and Technology of China. Her research interests include LPI radar signal detection and parameter estimation.
E-mail: 18804431003@163.com

TANG Bin was born in 1963. He is a professor of University of Electronic Science and Technology of China. His research interests include complex/combination modulation LPI and new system radar reconnaissance and interference technology, adaptive radar reconnaissance and interference technology, networked radar countermeasure technology, broadband/ultra-wideband radar digital reconnaissance receiving and interference technology.
E-mail: bint@uestc.edu.cn